INTERNATIONAL JOURNAL FOR NUMERICAL METHODS IN FLUIDS
Int. J. Numer. Meth. Fluids 2008; **57**:329–354
Published online 6 November 2007 in Wiley InterScience (www.interscience.wiley.com). DOI: 10.1002/fld.1637

Combined interface boundary condition method for coupled thermal simulations

B. Roe[1], R. Jaiman[1], A. Haselbacher[2] and P. H. Geubelle[1,*,†]

[1]*University of Illinois at Urbana-Champaign, Urbana, IL 61801, U.S.A.*
[2]*University of Florida, Gainesville, FL 32611, U.S.A.*

SUMMARY

A new procedure for modeling the conjugate heat-transfer process between fluid and structure subdomains is presented. The procedure relies on higher-order combined interface boundary conditions (CIBC) for improved accuracy and stability. Traditionally, continuity of temperature and heat flux along interfaces is satisfied through algebraic jump conditions in a staggered fashion. More specifically, Dirichlet temperature conditions are usually imposed on the fluid side and Neumann heat-flux conditions are imposed on the solid side for the stability of conventional sequential staggered procedure. In this type of treatment, the interface introduces additional stability constraints to the coupled thermal simulations. By utilizing the CIBC technique on the Dirichlet boundary conditions, a staggered procedure can be constructed with the same order of accuracy and stability as those of standalone computations. Using the Godunov–Ryabenkii normal-mode analysis, a range of values of the coupling parameter is found that yields a stable and accurate interface discretization. The effectiveness of the method is investigated by presenting and discussing performance evaluation data using a 1D finite-difference formulation for each subdomain. Copyright © 2007 John Wiley & Sons, Ltd.

Received 12 December 2006; Revised 30 August 2007; Accepted 6 September 2007

KEY WORDS: conjugate heat transfer; staggered procedure; combined interface boundary conditions; stability

1. INTRODUCTION

The thermal interaction between fluid and solid subdomains plays an important role in a wide range of multiphysics problems, such as heating of space vehicles in hypersonic flow [1], heating

*Correspondence to: P. H. Geubelle, Department of Aerospace Engineering, University of Illinois, 306 Talbot Lab, 104 S. Wright St., Urbana, IL 61801, U.S.A.
†E-mail: geubelle@uiuc.edu

Contract/grant sponsor: Center for Simulation of Advanced Rockets at the University of Illinois at Urbana-Champaign/Department of Energy through the University of California; contract/grant number: B523819

and cooling of turbine blades in jet engines [2], and thermoelastic deformation of a structure due to aerodynamic heating [3]. One way of modeling the above phenomena is to use a monolithic (i.e. tightly coupled) discretization for both solid and fluid subdomains with the interface boundary conditions [4, 5]. However, one generally solves different equations in the solid and fluid subdomains: Typically, the unsteady thermal diffusion equation is computed in the solid subdomain, and the Navier–Stokes equations supplemented by appropriate turbulence models are solved in the fluids subdomain. In addition, the discretization approaches are often different: Commonly, the finite-element method is used in the solid subdomain, whereas the finite-volume method is adopted in the fluid subdomain. These differences can lead to difficulties in developing a computationally efficient monolithic scheme.

A natural way of avoiding such difficulties is to solve the coupled thermal equations in a partitioned manner. In a partitioned solution procedure, the fluid and solid subdomains are solved sequentially on decomposed non-overlapping subdomains. A key component of a partitioned procedure is the formulation and implementation of the interface conditions characterizing the fluid–structure coupling. The fluid and structure equations are alternately integrated in time by separate solvers with the aid of Dirichlet and Neumann boundary conditions along the interface. This technique for solving coupled mechanical system was introduced by Felippa and Park [6], which is often referred to the conventional sequential staggered (CSS) procedure.

For conjugate heat-transfer problems without deformation, Giles [7] demonstrated that the fluid subdomain should be given a Dirichlet condition for temperature continuity, while the solid subdomain should be subjected to a Neumann condition for heat-flux continuity to maximize stability when both subdomains are discretized with finite-difference methods. As shown in [7, 8], the stability restriction of the CSS procedure is more restrictive than those of the individual subdomains. The stability analyses were conducted using the Godunov and Ryabenkii [9] method and the analytical results were verified numerically. In [8], special emphasis was placed on the effect of the interface motion on the stability limit for both finite-difference and finite-volume/finite-element discretizations of the fluid and solid subdomains. The results indicated that the stability properties of the explicit CSS procedure are strongly dependent on the interface characteristics, e.g. interface velocity, relative physical (e.g. mass density, heat capacities), and geometric properties (e.g. mesh size) along the interface. Additionally, the CSS scheme suffers from a time lag between the integration of the coupled thermal equations. This time lag leads to an artificial energy production, which may cause numerical instability in the coupled thermal simulations. A similar phenomenon has been observed in 1D model piston problem for fluid–structure interaction (FSI) in [10]. A special treatment is thus required to counteract energy production in the staggered scheme.

In this study, we present a new coupling scheme that reduces and eliminates stability constraints associated with the interface treatment, while preserving the explicit 'loosely coupled' nature of the solution procedure. The new coupling scheme, referred to as the combined interface boundary condition (CIBC) scheme, consists of partitioning the coupled subdomain and imposing interface conditions that relax the temperature continuity (Dirichlet) condition. Instead, higher-order corrections that are applied to obtain new interface values with appropriate compensation may counteract with the artificial energy production caused by the staggering process. A similar approach has been used in [11, 12] to show stability of linearized FSI using matching and non-matching meshes. To the best of our knowledge, this method has not been considered in any previous studies of transient conjugate heat-transfer problems. Our emphasis hereafter is to study the numerical stability and accuracy of the CIBC scheme with the aid of explicit 1D loosely coupled thermal system. A variant of the CIBC scheme has been developed and implemented for nonlinear FSI using unstructured

DOI: 10.1002/fld

finite-volume formulation in the fluid subdomain and finite-element discretization in the structural subdomain [13].

Of interest in this work is the 1D thermal diffusion problem with a moving interface described by

$$\rho C\frac{\partial T}{\partial t}+\rho C v_0\frac{\partial T}{\partial x}=-\frac{\partial q}{\partial x}\quad \text{with } q=-\kappa\frac{\partial T}{\partial x} \tag{1}$$

where $T(x,t)$ represents the temperature field, $q(x,t)$ is the heat flux, ρ is the density, C is the relevant specific heat, v_0 is the interface velocity, and κ is the thermal conductivity. The model equation (1) can be used to represent each subdomain, although the material parameters are discontinuous across the interface. Throughout this article, ρ, C, v_0, and κ are assumed to be constant in each subdomain. Each subdomain can represent either fluid or solid media.

Following the convention adopted by Giles [7], the subdomain that passed the Dirichlet condition is represented by $+$ subscripts, while the subdomain that passed the Neumann condition is represented by $-$ subscripts. Based on the results of [7, 8], the $+$ and $-$ subdomains should represent the fluid and solid, respectively, for maximum stability. Hence, the terms 'fluid subdomain' and '$+$ subdomain' are used interchangeably, and similarly for 'solid subdomain' and '$-$ subdomain'. For the fluid subdomain Ω_+, C is the specific heat at constant volume C_V. For the solid subdomain Ω_-, C is equal to the specific heat C_P. The boundary conditions as $x\to\pm\infty$ are that the temperature field asymptotes to constant values $T_{\pm\infty}$, and hence the heat flux tends to zero. At the interface Γ, the Dirichlet and Neumann continuity conditions are given by

$$T_+=T_-\quad \text{and}\quad q_+=q_- \tag{2}$$

We discretize both subdomains with the finite-difference technique. As discussed in [7], a stability analysis for this 1D coupled thermal model problem allows us to generate a necessary stability condition for more complex 2D and 3D computations.

The remainder of this article is organized as follows. Section 2 summarizes the CSS scheme, and the formulation and implementation of the CIBC method are described in Section 3. In Section 4, the stability of the CIBC scheme is analyzed using the Godunov–Ryabenkii theory. The stability analysis is verified numerically in Section 5, where results of an accuracy study are also reported.

2. CSS SCHEME

In partitioned staggered procedures, the fluid and solid thermal fields are commonly discretized in space by different schemes and integrated in time by a staggered numerical scheme (see Figure 1). A simple and popular partitioned procedure for solving conjugate heat-transfer problems is the CSS scheme [6] whose generic cycle is described in Algorithm 1. For simplicity, we first consider the particular case of a stationary interface for the 1D coupled thermal system, for which (1) takes the form

$$c\frac{\partial T}{\partial t}=-\frac{\partial q}{\partial x}\quad \text{with } q=-\kappa\frac{\partial T}{\partial x} \tag{3}$$

where $c=\rho C$. Most of the derivations and results summarized in this paper pertain to the stationary interface case, while the more complex moving interface problem is discussed in Section 5.2.

DOI: 10.1002/fld

Algorithm 1. Explicit CSS scheme for the coupled thermal problem

1. Start from initial temperature fields prescribed in both subdomains
2. Update temperature solution as follows:
   (a) Advance heat equation for solid (−) subdomain using known interface heat flux $q_{0_-}^n$

$$c_- \left.\frac{\partial T_-}{\partial t}\right|^n = -\left.\frac{\partial q_-}{\partial x}\right|^n \quad \text{in } \Omega_-$$

   (b) Impose Dirichlet condition on the interface boundary of fluid (+)

$$T_{0_+}^n = (1-\alpha)T_{0_-}^n + \alpha T_{0_-}^{n+1} \quad \text{on } \Gamma \text{ where } \alpha \in [0,1]$$

   (c) Advance heat equation for fluid (+) subdomain using known interface temperature $T_{0_+}^n$

$$c_+ \left.\frac{\partial T_+}{\partial t}\right|^n = -\left.\frac{\partial q_+}{\partial x}\right|^n \quad \text{in } \Omega_+$$

   (d) Extract interface heat flux $q_{0_+}^{n+1}$ and impose Neumann condition on the interface boundary of solid (−) subdomain

$$q_{0_-}^{n+1} = (1-\beta)q_{0_+}^n + \beta q_{0_+}^{n+1} \quad \text{on } \Gamma \text{ where } \beta \in [0,1]$$

In Algorithm 1, $|^n$ denotes the current time level for the derivatives, and α and β are weighting parameters to interpolate the interface solutions between the time levels n and $n+1$. In the case of $\alpha=0$ and $\beta=0$, the solutions at time level $n+1$ is ignored and the previous solution at time step n is transferred to the respective subdomains. This method is referred to a parallel conventional staggered method [6], since the fluid and structural subdomains can start their computations at the same time level and perform their inner subdomain integrations in a parallel way. When $\alpha=1$ and $\beta=1$, the CSS method described above is obtained. Selecting values between zero and one for α and β may result in an under-relaxed staggered scheme that usually introduces spurious dissipation to the coupled system.

For non-overlapping interfaces, the governing equation is not applied along the interface. Instead, the continuity conditions given by (2) are enforced sequentially. This time-stepping approach may suffer significantly from destabilizing effects introduced by the interface conditions. Instability associated with the interface may depend on relative physical and discretization parameters of the neighboring subdomains, e.g. heat capacity, density, mesh resolutions, and time steps. Moreover, due to obvious time lag between the Ω_+ and Ω_- computations, sequential staggered solution techniques can be only formally first-order accurate in time when no extrapolations are used, although the individual subdomains may be higher-order accurate.

For these reasons, it is often attempted to correct these deficiencies in partitioned loosely coupled framework by performing inner- or pseudo-iterations between each pair of consecutive

DOI: 10.1002/fld

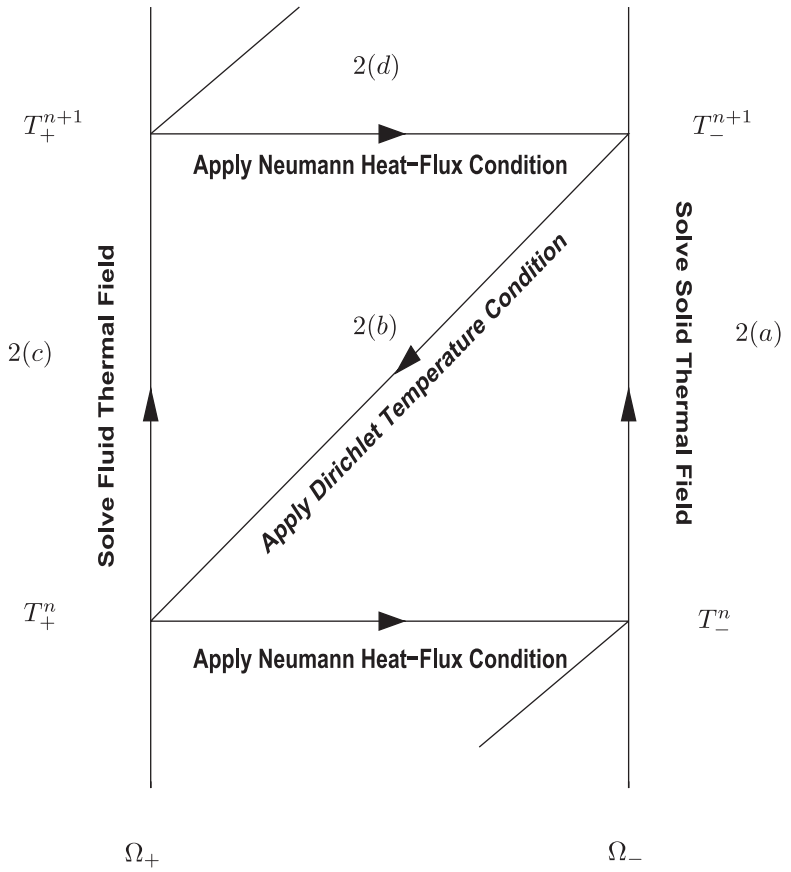

Figure 1. Schematic of conventional sequential staggered (CSS) scheme for $\alpha=1$ and $\beta=1$. Step labels 2(a)–(d) refer to Algorithm 1.

time stations. Sometimes such staggered procedures are referred to as strong coupling methods [14] in the literature of aeroelasticity. However, these pseudo-iterations increase the complexity of the implementation of conjugate heat-transfer analyses as well as the computational cost of each time step. These drawbacks of staggered methods motivate us to construct a new coupling procedure for improving information exchange across the interface, as described in the following section.

3. COMBINED INTERFACE BOUNDARY CONDITIONS METHOD

3.1. Overview

Owing to inherent flexibility in the partitioned loosely coupled method, it is relatively easy to construct various iterative coupling procedures at both the conceptual and algorithmic levels. However, it may be a challenging task to design a partitioned method that provides temporal accuracy and numerical stability. The CIBC approach achieves improved stability and precision by

DOI: 10.1002/fld

solving additional partial differential equations (PDEs) for the interface quantities based on their space and time derivatives.

The CIBC scheme shares features with the iterative interface relaxation procedure [15, 16], which involves a relaxation parameter and iterates the interface procedure at each pseudo-time step. In [15, 16], some guidelines are also given on the optimal choice of the relaxation parameter. As in interface relaxation procedures, the CIBC scheme involves a coupling parameter for combining the error in heat-flux rate (i.e. history effects) with the net heat-flux gradient with the goal of correcting the Dirichlet condition. The derivations presented in this section assume a non-moving interface, i.e. $v_0 = 0$. The more general case for which $v_0 \neq 0$ is discussed in Section 5.2.

3.2. Formulation and algorithm

In the conventional staggered scheme, the governing equation of each subdomain has no influence along the interface. Instead, the continuity of heat flux (Neumann condition) and temperature continuity (Dirichlet condition) given by (2) are enforced. By contrast, in the CIBC method formulation, the interface solution is influenced explicitly by the neighboring subdomains. For the coupled thermal problem, specific residual operators for the Dirichlet condition $\mathscr{R}^{\mathrm{D}}$ and Neumann condition $\mathscr{R}^{\mathrm{N}}$ are given by

$$\mathscr{R}^{\mathrm{D}}\left(\frac{\partial T_{0_-}}{\partial t}, \frac{\partial \mathbf{q}_{0_-}}{\partial t}, \frac{\partial \mathbf{q}_{0_+}}{\partial n}, \frac{\partial \mathbf{q}_{0_+}}{\partial t}\right) = 0, \quad \mathscr{R}^{\mathrm{N}}(\mathbf{q}_{0_+}, \mathbf{q}_{0_-}) = 0 \tag{4}$$

where $(\partial \mathbf{q}_{0_+}/\partial n)$ denotes the derivative of the fluid heat-flux $\mathbf{q}_{0_+}$ with respect to the outward normal $\mathbf{n}$ along the interface Γ. Based on the current solutions on both sides of the interface, these operators calculate successive corrections to the solution on the interface Γ. Although the coupling scheme described in [12] calls for corrections of both the Dirichlet and Neumann boundary conditions, the treatment described hereafter deals with the modification of the Dirichlet condition only. This approach is used because preliminary numerical tests demonstrated no additional stability enhancement if the Neumann boundary conditions were also modified. In fact, tests have shown that a CIBC approach that corrects both boundary conditions may exhibit worse stability characteristics than the one that corrects the Dirichlet condition or the Neumann condition separately at each time step. The reasons for this behavior are still under investigation.

The derivation of the residual $\mathscr{R}^{\mathrm{D}}$ for the CIBC scheme starts with the Dirichlet condition (2) for the fluid subdomain Ω_+, which can be differentiated with respect to time as

$$\frac{\partial T_{0_+}}{\partial t} = \frac{\partial T_{0_-}}{\partial t} \tag{5}$$

Expressing (3) for the interface gives

$$c_+ \frac{\partial T_{0_+}}{\partial t} = -\frac{\partial q_{0_+}}{\partial x} \tag{6}$$

where $c_\pm = \rho_\pm C_\pm$. Substituting (5) into (6) yields

$$c_+ \frac{\partial T_{0_-}}{\partial t} = -\frac{\partial q_{0_+}}{\partial x} \tag{7}$$

DOI: 10.1002/fld

Differentiating the Neumann condition for the solid subdomain Ω_- with respect to time, we obtain

$$\frac{\partial q_{0_-}}{\partial t} = \frac{\partial q_{0_+}}{\partial t} \tag{8}$$

By multiplying (8) with a dimensional coupling parameter ω with the units of time/length and adding the resulting equation to (7), we can write an expression for $\mathscr{R}^{\mathrm{D}}$ as

$$c_+ \frac{\partial T_{0_-}}{\partial t} + \frac{\partial q_{0_+}}{\partial x} + \omega \left(\frac{\partial q_{0_+}}{\partial t} - \frac{\partial q_{0_-}}{\partial t} \right) = 0 \tag{9}$$

While (8) is satisfied at the continuum level, it is not necessarily satisfied for the discrete coupled system based on the partitioned staggered procedure.

Relationship (9) provides an estimate for the temperature correction between the two successive time levels n and $n+1$. Instead of applying $T_{0_-}^{n+1}$ to the fluid subdomain as in the conventional staggered scheme, we apply a corrected temperature value

$$T_{0_*}^n = T_{0_-}^n + \delta T_{0_-}^n \tag{10}$$

where the temperature correction $\delta T_{0_-}^n$ is obtained by discretizing (9) as

$$\delta T_{0_-}^n = \frac{\Delta t}{c_+} \left[-\frac{\partial q_{0_+}^n}{\partial x} + \omega \left(\frac{\partial q_{0_-}^n}{\partial t} - \frac{\partial q_{0_+}^n}{\partial t} \right) \right] \tag{11}$$

In (11), $\partial/\partial x$ and $\partial/\partial t$ can be simply computed using first-order accurate difference approximations. Owing to the lack of local energy conservation in the staggered partitioned scheme compared with the monolithic scheme, there is a non-zero value of the temperature correction $\delta T_{0_-}^n$ at the discrete time level n. A detailed analysis is presented in Appendix A.

Since the standard Dirichlet condition has been used to derive this result, temperature continuity is still satisfied indirectly. Using (3) also ensures that the interface temperature solution satisfies the governing differential equation, which tends to improve both the accuracy and the stability of the interface discretization. Figure 2 illustrates the CIBC coupling algorithm for a coupled thermal simulation. This algorithm differs from the conventional staggered scheme only in the treatment of the Dirichlet boundary condition (10).

It is worth pointing out that since the CIBC method decomposes and combines interface boundary conditions at the continuum level, the convergence analysis for this coupling method can be carried out at the continuum level (i.e. in terms of PDEs) and therefore is a mathematical and not a numerical analysis problem. Such a stability analysis is carried out at the differential level using energy arguments in [12] for linearized FSI. There are several challenging questions, however, concerning practical applications of such methods, such as finding suitable values of the coupling parameter ω. In the following section, the stability of the CIBC method is analyzed using the Godunov–Ryabenkii method and suitable values of the coupling parameter are determined.

DOI: 10.1002/fld

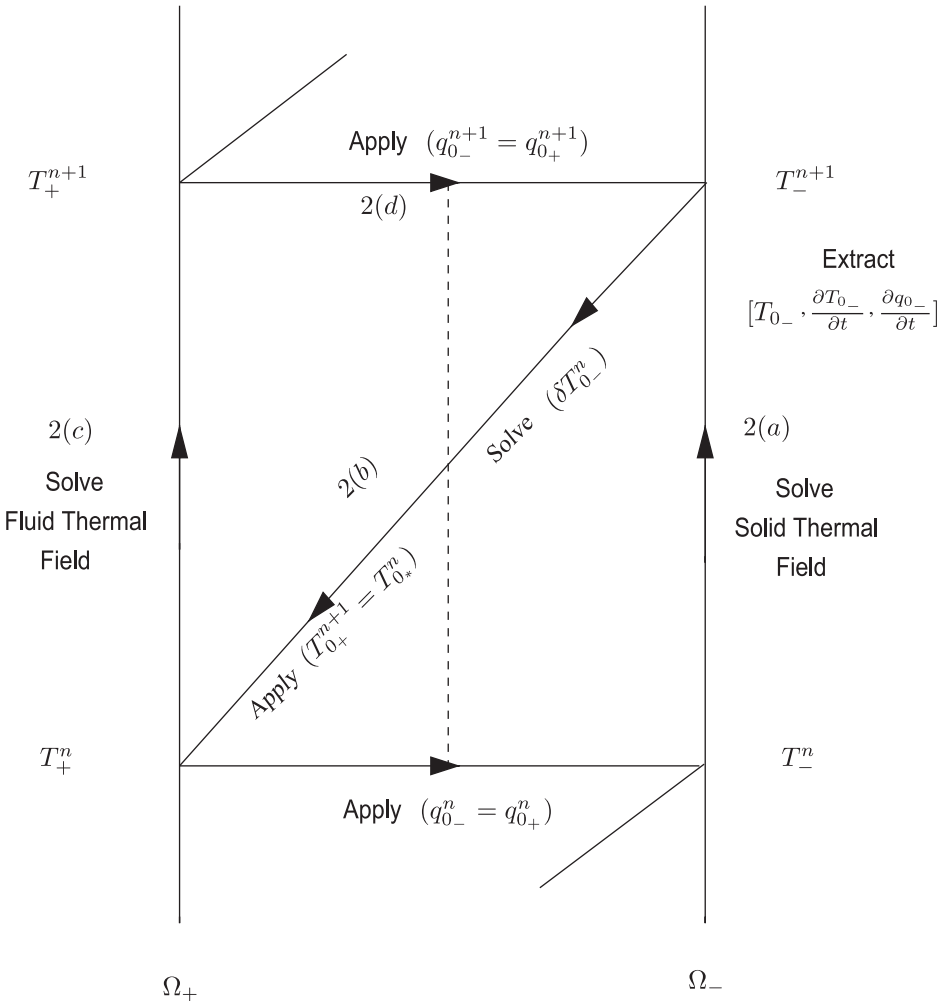

Figure 2. Schematic of the combined interface boundary conditions (CIBC) method. Step labels 2(a)–(d) refer to Algorithm 2.

3.3. Discretization

To approximate the model equation (3) by finite differences, we divide the composite subdomain $\bar{\mathbb{R}} \times [0, t_F]$ by a set of lines parallel to the x- and t-axes to form a space–time finite-difference grid. We shall assume that the sets of lines are equally spaced and write Δx and Δt for the line spacings. The derivatives in (3) are approximated by finite differences. For the model problem, the simplest difference scheme based at the mesh point (x_j, t_n) uses a forward difference for the time derivative and central difference for the second-order space derivative.

DOI: 10.1002/fld

Algorithm 2. Explicit combined interface boundary conditions method for the coupled thermal problem

1. Start from initial temperature fields prescribed in both subdomains.
2. Generate corrected interface temperature $T_{0_*}^n$ and new heat flux $q_{0_+}^{n+1}$ as follows:
   (a) Advance heat equation for solid $(-)$ subdomain

$$c_- \left.\frac{\partial T_-}{\partial t}\right|^n = -\left.\frac{\partial q_-}{\partial x}\right|^n \quad \text{in } \Omega_-$$

   (b) Compute interface temperature $T_{0_*}^n$ using (10) and transfer it to fluid $(+)$ subdomain

$$T_{0_+}^{n+1} = T_{0_*}^n = T_{0_-}^n + \frac{\Delta t}{c_+}\left[-\frac{\partial q_{0_+}^n}{\partial x} + \omega\left(\frac{\partial q_{0_-}^n}{\partial t} - \frac{\partial q_{0_+}^n}{\partial t}\right)\right] \quad \text{on } \Gamma \text{ where } \omega \geqslant 0$$

   (c) Advance heat equation for fluid $(+)$ subdomain

$$c_+ \left.\frac{\partial T_+}{\partial t}\right|^n = -\left.\frac{\partial q_+^n}{\partial x}\right|^n \quad \text{in } \Omega_+$$

   (d) Apply Neumann interface condition

$$q_{0_-}^{n+1} = q_{0_+}^{n+1} \quad \text{on } \Gamma$$

Figure 3 describes the spatial discretization with the node numbering and interface boundary conditions. By discretizing (3) in the $(-)$ subdomain $(x<0)$, we obtain

$$c_- \frac{T_j^{n+1} - T_j^n}{\Delta t} = \kappa_- \frac{T_{j+1}^n - 2T_j^n + T_{j-1}^n}{\Delta x_-^2} \quad (j = 0_-, -1, -2, -3, \ldots) \tag{12}$$

and, for the $(+)$ subdomain,

$$c_+ \frac{T_j^{n+1} - T_j^n}{\Delta t} = \kappa_+ \frac{T_{j+1}^n - 2T_j^n + T_{j-1}^n}{\Delta x_+^2} \quad (j = 1, 2, 3, \ldots) \tag{13}$$

In (12) and (13), Δt is the matching time step size for both subdomains, and T_j^n is given by

$$T_j^n = \begin{cases} T(j\Delta x_-, n\Delta t) & \text{if } j = 0, -1, -2, \ldots \\ T(j\Delta x_+, n\Delta t) & \text{if } j = 1, 2, 3, \ldots \end{cases} \tag{14}$$

From the initial and boundary values, we can calculate all the interior and interface values for successive values of n.

DOI: 10.1002/fld

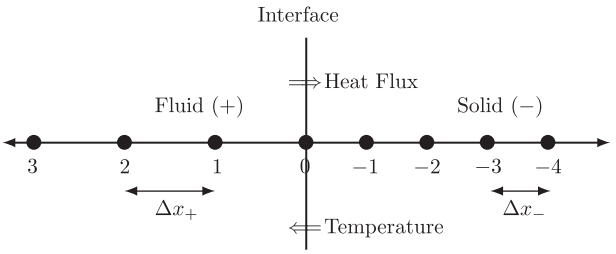

Figure 3. Schematic of discretized subdomain and node numbering.

For the interface boundary conditions, we apply the Neumann condition on the (−) subdomain and the Dirichlet condition on the (+) subdomain, as indicated in Figure 3. By discretizing (3) along the interface, we obtain

$$c_- \frac{T_{0_-}^{n+1} - T_{0_-}^n}{\Delta t} = \left(-q_+ - \kappa_- \frac{T_{0_-}^n - T_{-1}^n}{\Delta x_-} \right) \frac{2}{\Delta x_-} \tag{15}$$

where the heat flux q_+ is computed by a first-order approximation of the temperature gradient on the interface

$$q_+ = -\kappa_+ \left(\frac{T_1^n - T_{0_*}^n}{\Delta x_+} \right) \tag{16}$$

and it is transferred to the (−) subdomain as the Neumann boundary condition with the aid of the corrected temperature value T_0^*.

The fully discretized version of (10) is thus

$$\begin{aligned} T_{0_*}^n = T_{0_-}^n + \frac{\Delta t}{c_+} \Bigg(& \frac{\kappa_+}{\Delta x_+^2} (T_2^{n-1} - 2T_1^{n-1} + T_{0_+}^{n-1}) \\ & + \omega \left\{ \frac{\kappa_+}{\Delta x_+ \Delta t} [(T_1^{n-1} - T_{0_+}^{n-1}) - (T_1^{n-2} - T_{0_+}^{n-2})] \right. \\ & \left. - \frac{\kappa_-}{\Delta x_- \Delta t} [(T_{0_-}^n - T_{-1}^n) - (T_{0_-}^{n-1} - T_{-1}^{n-1})] \right\} \Bigg) \end{aligned} \tag{17}$$

Using the explicit update, the Dirichlet boundary condition to the fluid domain is set by the corrected interface temperature field $T_{0_*}^n$

$$T_{0_+}^{n+1} = T_{0_*}^n \tag{18}$$

DOI: 10.1002/fld

where T_{0_+} lags by T_{0_*} one iteration. Furthermore, combining (15)–(17) yields

$$T_{0_+}^{n+1} = T_{0_-}^{n} + \frac{2\Delta t}{c_-\Delta x_-}\left\{\frac{\kappa_+}{\Delta x_+}\left(T_1^n - T_{0_-}^n - \frac{\Delta t}{c_+}\left[\frac{\kappa_+}{\Delta x_+^2}(T_2^{n-1} - 2T_1^{n-1} + T_{0_+}^{n-1})\right.\right.\right.$$
$$+\omega\left\{\frac{\kappa_+}{\Delta x_+\Delta t}[(T_1^{n-1} - T_{0_+}^{n-1}) - (T_1^{n-2} - T_{0_+}^{n-2})]\right.$$
$$\left.\left.\left.-\frac{\kappa_-}{\Delta x_-\Delta t}[(T_{0_-}^{n} - T_{-1}^{n}) - (T_{0_-}^{n-1} - T_{-1}^{n-1})]\right\}\right]\right) - \frac{\kappa_-}{\Delta x_-}[T_{0_-}^n - T_{-1}^n]\right\} \tag{19}$$

The more general case involving interface motion is analyzed in Appendix B.

4. GODUNOV–RYABENKII STABILITY ANALYSIS

The stability analysis relies on the normal-mode representation, which generalizes further the matrix method by replacing it with local modes as a power series of quasi-eigenvectors [9]. This constitutes a property for local analysis of the influence of boundary conditions as opposed to the von Neumann analysis, which requires periodic conditions. In addition, it allows us to derive exact solutions of the difference schemes and permits the analysis of the error propagation through the space mesh.

As in [7, 8], we now apply the stability theory of Godunov–Ryabenkii [9, 17] to examine the existence of separable normal modes of the form at node point i and time step n:

$$T_j^n = \begin{cases} z^n k_-^j & \text{if } j \leqslant 0 \\ z^n k_+^j & \text{if } j > 0 \end{cases} \tag{20}$$

for the difference equations (12), (13), and (19), where z is the time-amplification factor and k is the space-amplification factor. When introduced into a numerical scheme formed by the interior scheme and the interface conditions, we obtain a set of characteristic equations that couples the time-amplification factor z with the space-amplification factor k.

The theory states that the interior scheme needs to be von Neumann stable in a domain and a mode k^j with $|k|>1$ will lead to an unbounded solution in space, which means that k^j will increase without bound when j goes to infinity. Therefore, $|k|$ should be less than one, and the necessary condition states that all the modes with $|k|\leqslant 1$ produced by the interface boundary conditions should correspond to $|z|<1$.

Let us now define the following non-dimensional parameters:

$$r \equiv \frac{c_+\Delta x_+}{c_-\Delta x_-} \tag{21}$$

$$d_\pm \equiv \frac{\kappa_\pm \Delta t}{c_\pm \Delta x_\pm^2} \tag{22}$$

DOI: 10.1002/fld

and

$$\theta_{\pm} \equiv \frac{\kappa_{\pm}\omega}{c_{\pm}\Delta x_{\pm}} \tag{23}$$

The parameters defined by (21) and (22) are equal to those used in [7, 8]. The parameters defined by (23), which contain the coupling parameter ω, arise due to the CIBC treatment of the interface coupling.

Solving (12) for T_j^{n+1} and applying the dimensionless parameter d_-, we obtain

$$T_j^{n+1} = T_j^n + d_-(T_{j+1}^n - 2T_j^n + T_{j-1}^n) \tag{24}$$

Substituting (20) into (24), the characteristic equation becomes

$$z = 1 + d_-(k_- - 2 + k_-^{-1}) \tag{25}$$

in the $(-)$ subdomain. Similarly, for the $(+)$ subdomain, we obtain the characteristic equation

$$z = 1 + d_+(k_+ - 2 + k_+^{-1}) \tag{26}$$

The discretized interface relation (19) can be rewritten as

$$\begin{aligned} T_{0_+}^{n+1} = T_{0_-}^n + 2rd_+ \Bigg[& T_1^n - T_{0_+}^n - \theta_+(T_1^{n-1} - T_{0_+}^{n-1} - T_1^{n-2} + T_{0_+}^{n-2}) \\ & + \frac{d_-\theta_+}{d_+ r}(T_{0_-}^n - T_{-1}^n - T_{0_-}^{n-1} + T_{-1}^{n-1}) - d_+(T_2^{n-1} - 2T_1^{n-1} + T_{0_-}^{n-1}) \Bigg] \\ & - 2d_-(T_{0_-}^n - T_{-1}^n) \end{aligned} \tag{27}$$

by substituting the non-dimensional parameters d_+, d_-, θ_+, and r. Applying (20) to (27) yields the characteristic relation

$$\begin{aligned} z = 1 + 2rd_+ & [(k_+ - 1) - \theta_+(k_+ - 1)(z^{-1} - z^{-2}) \\ & - z^{-1}d_+(k_+^2 - 2k_+ + 1)] + 2d_-(1 - k_-^{-1})[\theta_+(1 - z^{-1}) - 1] \end{aligned} \tag{28}$$

The interface stability relation is then obtained by solving (25) and (26) for k_- and k_+, respectively, and substituting the results into (28). k_- is given by

$$k_-^{-1} = 1 - \frac{1-z}{2d_-}\left(1 \mp \sqrt{1 - \frac{4d_-}{1-z}}\right) \tag{29}$$

Similarly, the solution for k_+ is

$$k_+ = 1 - \frac{1-z}{2d_+}\left(1 \mp \sqrt{1 - \frac{4d_+}{1-z}}\right) \tag{30}$$

DOI: 10.1002/fld

As stated earlier, to ensure stability as $j \to \pm\infty$, $|k_+|<1$ and $|k_-|>1$. These requirements are fulfilled by taking the negative signs in (29) and (30). Hence, we obtain

$$\begin{aligned} z = 1-2rd_+ &\left[\frac{1-z}{2d_+}\left(1-\sqrt{1-\frac{4d_+}{1-z}}\right)\right] \\ &\times\left\{1-\theta_+\left(\frac{1}{z}-\frac{1}{z^2}\right)+z^{-1}d_+\left[\frac{1-z}{2d_+}\left(1-\sqrt{1-\frac{4d_+}{1-z}}\right)\right]\right\} \\ &+2d_-\left[\frac{1-z}{2d_-}\left(1-\sqrt{1-\frac{4d_-}{1-z}}\right)\right]\left[\theta_+\left(1-\frac{1}{z}\right)-1\right] \end{aligned} \tag{31}$$

which can be solved for r as

$$r=\frac{z-1-2d_-\left[\frac{1-z}{2d_-}\left(1-\sqrt{1-\frac{4d_-}{1-z}}\right)\right][\theta_+(1-z^{-1})-1]}{-2d_+\left[\frac{1-z}{2d_+}\left(1-\sqrt{1-\frac{4d_+}{1-z}}\right)\right]\left\{1-\theta_+(z^{-1}-z^{-2})+z^{-1}d_+\left[\frac{1-z}{2d_+}\left(1-\sqrt{1-\frac{4d_+}{1-z}}\right)\right]\right\}} \tag{32}$$

The requirement for stability is $|z|<1$. The solution $z=1$ yields trivial solution in (32). By setting $z=-1$ in (32), we arrive at the following analytical stability criterion for the CIBC scheme:

$$r<\frac{\sqrt{1-2d_-}(1-2\theta_+)+2\theta_+}{(1-\sqrt{1-2d_+})(2\theta_++\sqrt{1-2d_+})} \tag{33}$$

Note that setting $\theta_+=0$ does not cause (33) to revert to the stability criterion of the CSS scheme given by [7]. This can be simply explained from (10), where setting $\omega=0$ leads to

$$T_{0_*}^n = T_{0_-}^{n+1}+\frac{\Delta t}{c_+}\frac{\partial q_+^n}{\partial x} \tag{34}$$

There are two points to be made about (33). Firstly, the terms multiplied by ω represent information from the interface history, while the heat-flux gradient term appearing in (33) is essentially a higher-order spatial term that remains even when $\omega=0$. Secondly, if we set $d_+=d_-=0.5$, which corresponds to the maximum time step size allowed by the Courant–Friedrichs–Lewy (CFL) condition in the fluid and solid subdomains, the stability criterion reduces to $r<1$ and is completely independent of d_+, d_-, and ω.

5. NUMERICAL RESULTS AND DISCUSSION

To assess the stability and precision of the CIBC coupling scheme and the accuracy of the analytical stability criterion derived in the previous section, we present results of a 1D numerical study performed with a coupled finite-difference thermal solver. The finite-difference equations are consistent with the formulation used for deriving (33).

DOI: 10.1002/fld

The model test problem specifies a uniform temperature in each domain, 1 K in the fluid subdomain and 0 K in the solid subdomain. At time $t=0$, the fluid subdomain is updated with T_{0_-} from the solid subdomain, producing the heat flux, q_+. After the first time step, T_{0_*}, defined by (10), is computed and used for updating the fluid subdomain (see Algorithm 2). The numerical results obtained with the CIBC coupling scheme are compared with those obtained with the traditional staggered scheme presented in Algorithm 1 with $\alpha=1$ and $\beta=1$.

Each subdomain is 1 m in length ($l_+=l_-=1$), and we use 200 equally distributed grid points to discretize both the subdomains. In addition, all the computations use the following parameters:

- specific heat capacities (J/m^3 K), $c_+=1000$, $c_-=2000$;
- thermal conductivities (W/m K), $\kappa_+=0.1$, $\kappa_-=0.2$;
- non-dimensional final time $t_F^*=(t_F\kappa_+/c_+l_+^2)=(t_F\kappa_-/c_-l_-^2)=0.1$.

5.1. Non-moving interface

5.1.1. Stability assessment. Figure 4(a) shows the maximum value of d_+ for which a stable solution can be maintained as the coupling parameter ω changes. Here, r is chosen as 1 and d_- varies from 0.35 to 0.5. In the figure, analytical stability limits obtained from (33) are denoted by the thicker curves, the numerical results are given by symbols, and the analytical stability limits corresponding to the conventional staggered scheme [8] are indicated by the thinner horizontal curves.

Four comments can be made about these results. First, the analytical and numerical stability limits match very well for all cases shown here. Second, in all cases, the stability limits imposed by the CIBC scheme are less restrictive than those corresponding to the conventional staggered coupling method. Third, when the non-dimensional coupling parameter θ_+ is less than roughly 0.5, the simulation remains stable even when $d_+=0.5$, which is in fact the CFL limit of the fluid (+) subdomain. For $\theta_+>0.5$, the maximum d_+ allowed decreases, yet remains significantly larger than that allowed when using the traditional coupling algorithm (thinner horizontal lines). Finally, the figure shows that, as d_- increases from 0.35 to 0.5, the rate at which the critical value of d_+ decreases from 0.5 is reduced. It seems counterintuitive that increasing d_- should correspondingly increase the critical value of d_+, but this occurs due to the problem approaching the scenario in which $d_+=d_-=0.5$, where, as stated in Section 4, the stability criterion reduces to $r<1$.

Similar conclusions can be reached from the results shown in Figure 4(b). However, θ_+ has the opposite effect on the critical value of d_- as it did on d_+. That is, $d_-=0.5$ gives a stable solution when θ_+ is equal to or larger than about 0.3, and decreases when θ_+ falls below this value. Again we see that, when $d_+=0.5$, the critical value of d_- is also 0.5. Unlike in the case of Figure 4(a), however, there is not an obvious pattern in the effect of decreasing d_+ from 0.5 where $\theta_+<0.3$. In all cases, the stability criterion still accurately predicts the critical value of d_-. Again, the curve corresponding to the conventional staggered scheme shows that $d_{-_{\text{crit}}}$ is smaller than that observed with the CIBC scheme. For clarity, only the conventional staggered scheme curve that represents the maximum value of $d_{-_{\text{crit}}}$ is shown.

Figures 4(c) and (d) are similar to Figures 4(a) and (b), respectively, except that $r=0.75$. The two figures are qualitatively identical to their $r=1$ counterparts, although here the numerical values of $d_{+_{\text{crit}}}$ and $d_{-_{\text{crit}}}$ have increased and the point at which θ_+ is able to maintain stability at 0.5 has shifted from 0.5 and 0.3 to 0.9 and 0.15, respectively. As before, the results produced by the CIBC method are more stable than those of the conventional staggered method for the range of coupling parameter θ_+ shown.

DOI: 10.1002/fld

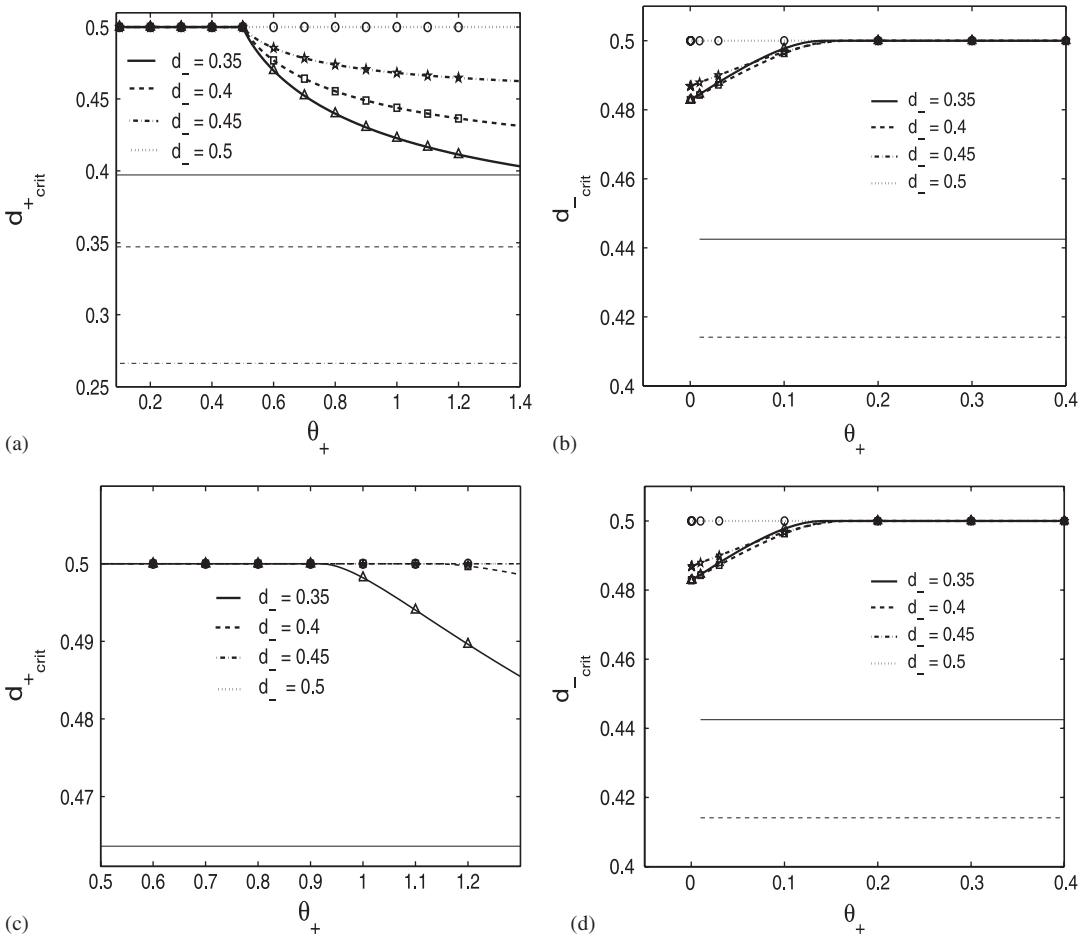

Figure 4. Effect of the non-dimensional coupling parameter θ_+ on the stability of the coupled scheme, i.e. on the critical values of d_+ and d_- beyond which instability occurs. (a) and (b): $r=1$; (c) and (d): $r=0.75$. The curves and symbols, respectively, denote the analytical and numerical solutions of the CIBC scheme, while the thinner horizontal lines correspond to the stability limit of the conventional staggered scheme.

It was stated previously that, when $d_+=d_-=0.5$, the stability criterion becomes $r<1$. Indeed, as shown in Figure 5(a), a simulation in which $d_+=d_-=0.5$ and $r=1$ seem to be neutrally stable. When $r<1$, the simulation becomes stable, as shown in Figure 5(b), for which $r=0.99$. It should be pointed out that $r=1$ is not a stringent stability limit since previous studies [7, 8] have shown that the coupling algorithm should always be arranged such that the fluid subdomain is given a Dirichlet condition and the solid subdomain a Neumann condition. In this case, for similar mesh spacings, r is always less than unity.

Figure 6(a) shows the region of stability for various values of r for the conventional staggered scheme. These results are compared with the results of the CIBC scheme shown in Figure 6(b). While the stability zone of the conventional staggered algorithm only fills the entire region of

DOI: 10.1002/fld

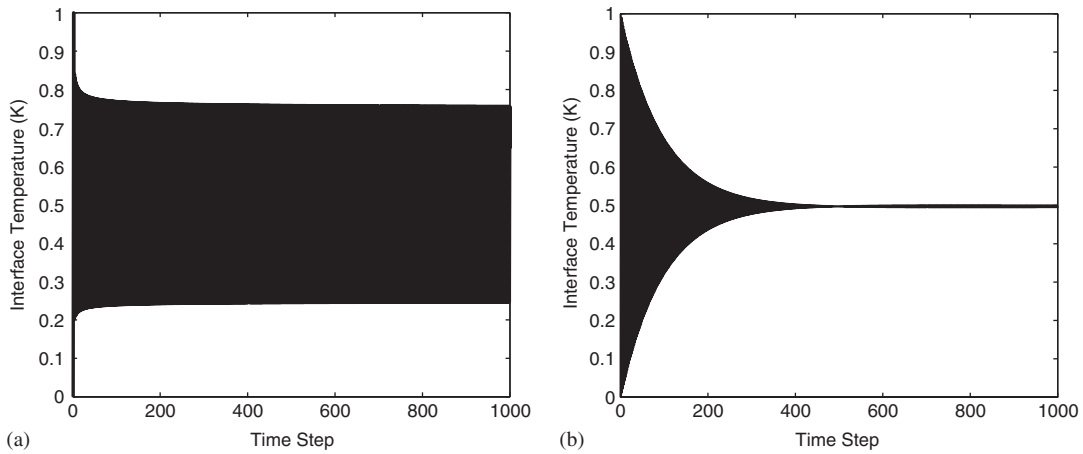

Figure 5. Interface temperature evolution where $d_+ = d_- = 0.5$ and $\theta_+ = 0.5$: (a) $r = 1$ and (b) $r = 0.99$.

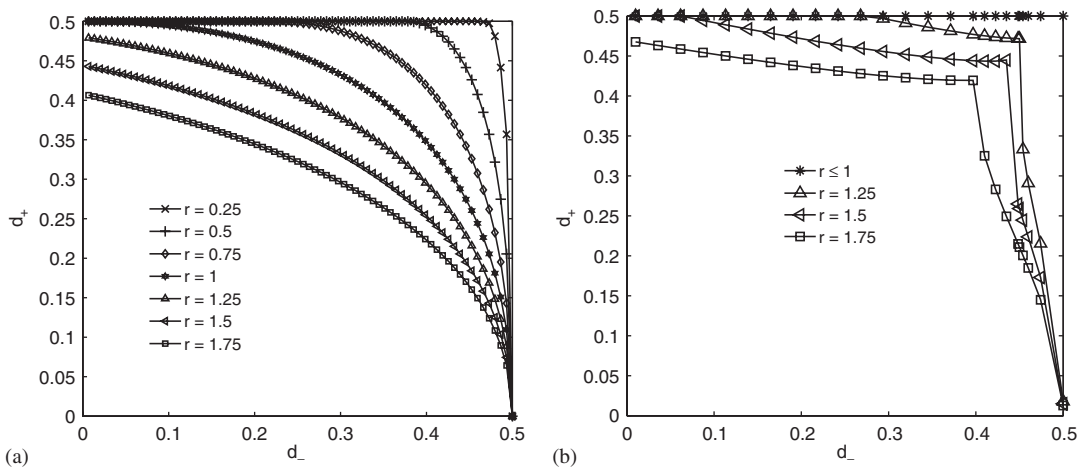

Figure 6. Effect of r on the predicted stability zones, with the stability regions lying below the curves: (a) conventional staggered scheme and (b) CIBC with $\theta_+ = 0.5$.

potential stability as $r \to \infty$, Figure 6(b) shows that the CIBC scheme requires only that $r < 1$ to reach that scenario. As r increases from 1, the size of the stability zone shrinks for the CIBC scheme, as it does for the conventional staggered scheme. Further, the figure illustrates that, for the range of r considered and $\theta_+ = 0.5$, the CIBC scheme is more stable than the CSS scheme.

The results presented above lead to the following conclusions: Firstly, the CIBC scheme allows the thermal FSI simulation to operate under conditions beyond the stability limit of the conventional staggered scheme. Secondly, if $r < 1$, the problem is stable when $d_+ = d_- = 0.5$, regardless of the choice of θ_+. When this is not the case, not all choices of θ_+ are equally suitable. Thirdly, if $r = 1$, optimal values of θ_+ from the point of view of stability seem to lie between 0.3 and 0.5.

DOI: 10.1002/fld

5.1.2. Accuracy assessment. We now turn our attention to the issue of accuracy of the new coupling scheme, and, in particular, on the effect of the coupling parameter on the precision of the numerical solution.

To quantify the accuracy of the coupling algorithm, we compare the numerical solution with the exact temperature field for two semi-infinite subdomains given by [18]

$$T_+(x,t)=\frac{\kappa_+\alpha_{D_+}^{-1/2}T_{i_+}}{\kappa_+\alpha_{D_+}^{-1/2}+\kappa_-\alpha_{D_-}^{-1/2}}\left[1+\frac{\kappa_-\alpha_{D_-}^{-1/2}}{\kappa_+\alpha_{D_+}^{-1/2}}\operatorname{erf}\left(\frac{x}{2\sqrt{\alpha_{D_+}t}}\right)\right] \tag{35}$$

and

$$T_-(x,t)=\frac{\kappa_+\alpha_{D_+}^{-1/2}T_{i_+}}{\kappa_+\alpha_{D_+}^{-1/2}+\kappa_-\alpha_{D_-}^{-1/2}}\operatorname{erfc}\left(\frac{|x|}{2\sqrt{\alpha_{D_-}t}}\right) \tag{36}$$

where $\alpha_{D_\pm}=\kappa_\pm/c_\pm$ and T_{i_+} is the initial temperature of the (+) subdomain, which, for our test problem, is chosen as 1 K. The exact interface temperature is thus given by

$$T_0^{\mathrm{ex}}=\frac{\kappa_+\alpha_{D_+}^{-1/2}T_{i_+}}{\kappa_+\alpha_{D_+}^{-1/2}+\kappa_-\alpha_{D_-}^{-1/2}} \tag{37}$$

To quantify the error incurred in simulations with the CSS and CIBC schemes, we take the L_2-norm of the computed interface temperature with respect to its analytical value,

$$\varepsilon_{T_0}(t_F^*)=\sqrt{\frac{\sum_{k=1}^{n(t_F^*)}(T_{0_{\mathrm{num}}}^k-T_{0_{\mathrm{ex}}}^k)^2}{\sum_{k=1}^{n(t_F^*)}(T_{0_{\mathrm{ex}}}^k)^2}} \tag{38}$$

where $n(t_F^*)$ is the number of time steps between $t=0$ and $t=t_F^*$, and $T_{0_k}^{\mathrm{num}}$ and $T_{0_k}^{\mathrm{ex}}$ refer to the numerical and exact interface temperatures at time step k.

Figure 7 shows the effect of θ_+ on the interface error. In all cases, the error appears to be increasing with $\theta_+\geqslant 0.5$ and, correspondingly, decreasing with d_+ and d_-, which is expected. However, each value of $d_\pm$ has an optimal value of θ_+ to minimize interface discretization error. In general, the optimal range of θ_+ is $0.1<\theta_+<0.5$.

In Figure 8(a), ε_{T_0} is given for both the CIBC and conventional staggered schemes. For the CIBC scheme, we set $\theta_+=0.5$ and results are shown for $d_+=d_-=0.25$, 0.4, and 0.5. On the other hand, for the conventional staggered scheme only the results for the $d_+=d_-=0.25$ case are shown, as it is unstable for the other two values. Considering first the $d_+=d_-=0.25$ case, for which a direct comparison can be made, we note that the CIBC scheme produces slightly more accurate results for most values of r. When r is greater than roughly 0.8, the conventional staggered algorithm is slightly more accurate. Again, increasing d_+ and d_- produces an expected increase in error, which for both cases is larger than either algorithm operating at $d_+=d_-=0.25$. Further, Figure 8(b) shows significant improvements in the interface accuracy, up to almost a factor of 2 for some values of r, for $\theta_+=0.25$.

Another aspect of the CIBC algorithm and that requires study is the order of temporal convergence. To that effect, we analyze the computation of ε_{T_0} at the interface for various time step sizes by varying $d_\pm$. Since material properties and grid spacings are held fixed for all cases,

DOI: 10.1002/fld

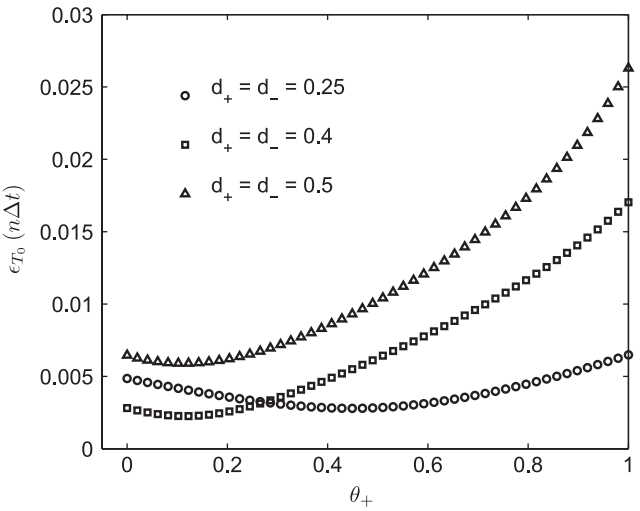

Figure 7. Effect of coupling parameter θ_+ on the interface error for $d_+ = d_- = 0.25$, 0.4, and 0.5, $r = 1$ and $n = 500$.

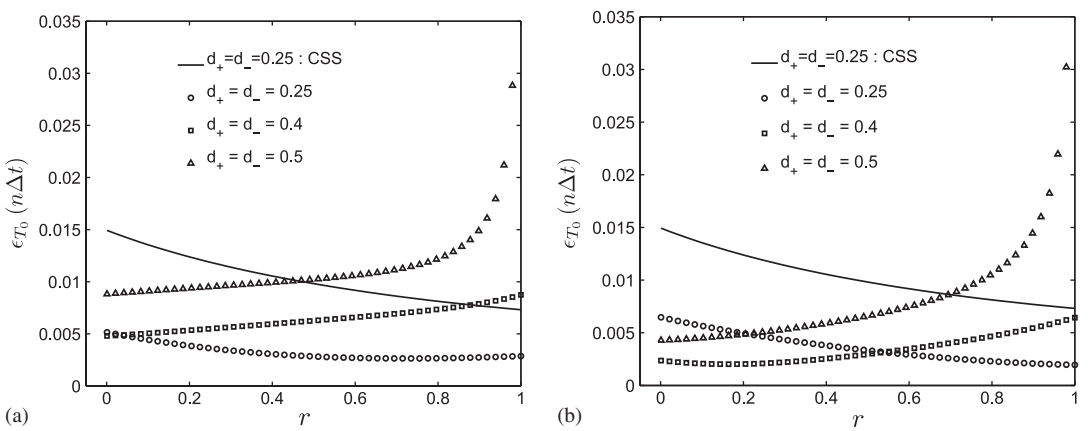

Figure 8. Comparison of error produced from the simulations using the CIBC (symbols) and the conventional staggered scheme (solid curve) as r is varied and $n = 500$: (a) $\theta_+ = 0.5$ and (b) $\theta_+ = 0.25$.

changes in the error are a direct result of varying the time step. Figures 9(a) and (b) show the results of a temporal convergence study for $r = 0.5$ and 1.0, respectively. For the CIBC scheme, the measured slope of ε_{T_0} is consistently higher than 2 for the three values of θ_+ considered, i.e. $\theta_+ = \{0.5, 0.25, 0.125\}$. The lowest value of $\theta_+ = 0.125$ shows an order of accuracy greater than 4, which suggests that the temporal convergence rate can be controlled by varying the coupling parameter. However, it is important to keep in mind that a lower limit is placed on θ_+ by the stability requirements presented in Figures 4(b) and (d).

DOI: 10.1002/fld

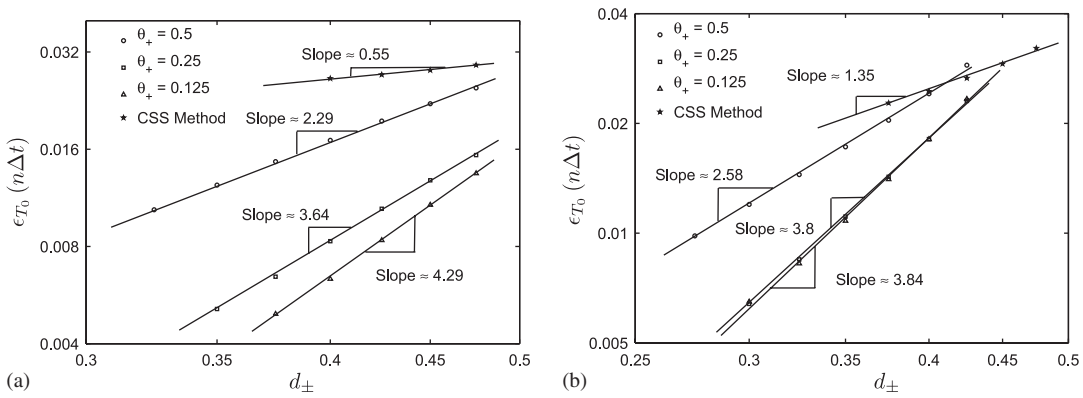

Figure 9. Dependence of the L_2-norm of the interface error at t_F^* for time step refinement at $n=500$: (a) $r=0.5$ and (b) $r=1.0$.

Indeed, the convergence rate of the CIBC scheme is substantially higher than that provided by the CSS scheme and individual subdomains. For this particular case, the CSS scheme has the order of accuracy of 0.55 for $r=0.5$ and 1.35 for $r=1.0$. The temporal convergence rate for an individual subdomain is about 1.0, which is expected for the forward Euler integration scheme. Furthermore, the two figures together show that there is a significant effect of the parameter r on the local temporal convergence rate, which implies that the local energy conservation error is dependent on the ratio of physical and geometric properties across the interface.

5.2. *Moving interface*

The precision and stability analysis presented above for a non-moving interface can be extended to the case of a moving interface. The main steps of the derivation are presented in Appendix B, and the key results are shown in Figure 10, which presents the v_0 dependence of the critical time step size for the CSS and CIBC schemes. The critical time step Δt_c beyond which instability occurs is normalized by the corresponding critical time step Δt_0 for the stationary interface given by (32). The curves correspond to the analytical prediction of Equation (B17) for the CIBC scheme and Equation (23) from [8] for the CSS scheme, while the symbols denote the numerical values obtained with the CIBC scheme.

As apparent in Figure 10, the interface velocity can have a substantial impact on the stability of the numerical solution of the coupled problem. The stability limit of the CIBC method is consistent with the CFL condition determined by Roe [8] as

$$d_\pm = \frac{(2-\eta_\pm)^2}{8} \tag{39}$$

where $\eta_\pm \equiv v_0 \Delta t / \Delta x_\pm$. However, the stability of the CSS scheme suffers from a larger negative impact of the interface motion. To retain stability, the CSS scheme may require a decrease in the time step size of up to an order of magnitude for a given value of the interface velocity. For the whole range of coupling parameters, the CIBC scheme is able to eliminate completely the instability associated with the interface discretization while operating at the CFL condition of both subdomains.

DOI: 10.1002/fld

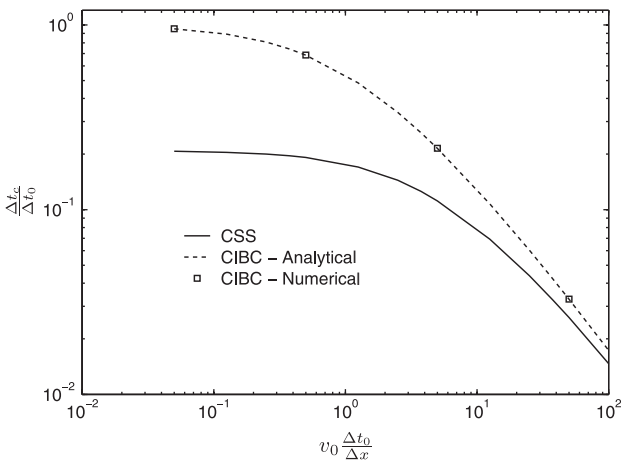

Figure 10. Effect of the interface velocity v_0 on the critical time step size. Δt_0 denotes the critical value of the time step for a non-moving interface as described by (32), with $r=1$ and $\theta_+=0.5$.

Although the analyses were performed here for the 1D model diffusion equation, the results are expected to be applicable to more complex situations in which the 2D and 3D diffusion equation is used to model the heat flux in the structure and the 2D/3D Navier–Stokes equations are used to model the behavior of the fluid.

6. CONCLUSION

Typical solution methods for conjugate heat-transfer problems update the temperature field in each subdomain by passing the fluid subdomain a temperature (Dirichlet) condition and the solid subdomain a heat-flux (Neumann) condition. This explicit coupling scheme is simple to implement and can be effective. However, it suffers from the important disadvantage that the coupling introduces a stability limit that is more restrictive than that of the two subdomains. In this paper, a new coupling scheme for the conjugate heat-transfer problem was introduced that reduces or eliminates this additional stability limit. The new coupling scheme consists of solving an additional PDE on the interface. This additional equation is derived from the Dirichlet and Neumann conditions at the interface and the governing equations in one of the subdomains and is therefore termed the combined interface boundary condition (CIBC) method. The additional equation contains a coupling parameter ω and is solved for a correction to the predicted interface temperature.

The Godunov–Ryabenkii method was used to analyze the stability properties of the CIBC method. The results of the stability analysis were verified using numerical tests. These tests showed that by careful selection of ω the stability zone of the coupled problem can be expanded such that only the CFL condition of each subdomain limits the stability of the problem. The optimal value of the non-dimensional coupling parameter, θ_+, seems to be approximately 0.1–0.5.

In addition to stability, the issue of accuracy of the coupled thermal algorithm was addressed. By comparing with an analytical solution, we verified that, in many cases, the CIBC scheme is not only more stable but also more accurate than the CSS method. Furthermore, convergence studies showed

DOI: 10.1002/fld

that the CIBC method results in an interface temperature that has a temporal convergence rate greater than 2, in contrast to the CSS schemes, which tend to achieve only first-order convergence.

APPENDIX A: MONOLITHIC *VS* PARTITIONED SCHEMES

To derive the comparison of the interface treatments between the monolithic and partitioned staggered schemes, we examine initial-value coupled thermal problem (3) using the finite-difference technique. In the monolithic discretization, using forward Euler time differencing and conservative spatial differencing based on the integral form of the unsteady thermal equation on the interval $x_{j-1/2} \leqslant x \leqslant x_{j+1/2}$ gives

$$C_j(T_j^{n+1} - T_j^n) = -(q_{j+1/2}^n - q_{j-1/2}^n) \tag{A1}$$

where $q_{j+1/2}^n = -K_{j+1/2}(T_{j+1}^n - T_j^n)$ with

$$K_{j+1/2} = \begin{cases} \kappa_-/\Delta x_-, & j+\frac{1}{2} < 0 \\ \kappa_+/\Delta x_+, & j+\frac{1}{2} > 0 \end{cases}$$

and

$$C_j = \begin{cases} c_-\Delta x_-/\Delta t, & j < 0 \\ \frac{1}{2}(c_-\Delta x_-/\Delta t + c_+\Delta x_+/\Delta t), & j = 0 \\ c_+\Delta x_+/\Delta t, & j > 0 \end{cases}$$

The interface continuity conditions are embedded implicitly in the governing equations with the two-sided approximations for the heat flux. This discretization is unconditionally stable from the viewpoint of interface treatment, i.e. the interface does not introduce any stability constraints [7].

In the partitioned staggered scheme, each part of the domain is solved independently with the information from the other subdomain. Thus, for given solutions at time level n in both subdomains, the explicit numerical algorithm for determining T_j^{n+1} is with the heat-flux data for the $(-)$ domain and the temperature data for the $(+)$ domain

$$\begin{aligned} c_- \frac{T_j^{n+1} - T_j^n}{\Delta t} &= \kappa_- \frac{T_{j+1}^n - 2T_j^n + T_{j-1}^n}{\Delta x_-^2}, \quad j < 0 \\ c_+ \frac{T_j^{n+1} - T_j^n}{\Delta t} &= \kappa_+ \frac{T_{j+1}^n - 2T_j^n + T_{j-1}^n}{\Delta x_+^2}, \quad j > 0 \end{aligned} \tag{A2}$$

At the interface point '0', the discretized heat-flux continuity relation takes the form

$$\frac{c_-\Delta x_-}{2}\left(\frac{T_0^{n+1} - T_0^n}{\Delta t}\right) = \underbrace{\kappa_+ \frac{T_1^n - T_0^n}{\Delta x_+}}_{-q_I} - \kappa_- \frac{T_0^n - T_{-1}^n}{\Delta x_-} \tag{A3}$$

DOI: 10.1002/fld

while the temperature continuity condition reads

$$T_0^n = T_I \tag{A4}$$

where the Neumann quantity q_I is computed from the one-sided approximation with the first-order accuracy at the interface of the (+) domain and the Dirichlet quantity T_I is directly applied from the (−) domain. From (A1) and (A3), it is clear that the partitioned scheme ignores the quantity $c_+\Delta x_+/2\Delta t$ due to the one-sided biasing in the interface computation. If $(c_+\Delta x_+/2\Delta t) \gg (c_-\Delta x_-/2\Delta t)$, this leads to a large partitioning error in the form of interface residual thermal energy. Consequently, the partitioned staggered scheme is conditionally stable and the stability depends on the relative physical and discretization parameters. The Godunov–Ryabenkii's stability theory quantifies the propagation of instability modes associated with the partitioning error between the two consecutive time steps for a range of r.

This analysis clearly indicates that appropriate compensation to the partitioning error is required. The CIBC method achieves that compensation by constructing an interface differential operator with the aid of the dimensional coupling parameter ω.

APPENDIX B: ANALYTICAL STABILITY LIMIT OF THERMAL MOVING INTERFACE

As mentioned previously, the subdomains are discretized with a finite-difference scheme: forward difference in time, a backward difference for the first spatial derivative, and a centered difference for the second spatial derivative.

In the (−) subdomain ($x < v_0 t$), the discretized version of (1) is

$$c_- \frac{T_j^{n+1} - T_j^n}{\Delta t} + c_- v_0 \frac{T_j^n - T_{j-1}^n}{\Delta x_-} = \kappa_- \frac{T_{j+1}^n - 2T_j^n + T_{j-1}^n}{\Delta x_-^2} \quad (j = 0_-, -1, -2, -3, \ldots) \tag{B1}$$

and the (+) subdomain ($x > v_0 t$), (1) takes the similar form

$$c_+ \frac{T_j^{n+1} - T_j^n}{\Delta t} + c_+ v_0 \frac{T_j^n - T_{j-1}^n}{\Delta x_+} = \kappa_+ \frac{T_{j+1}^n - 2T_j^n + T_{j-1}^n}{\Delta x_+^2} \quad (j = 1, 2, 3, \ldots) \tag{B2}$$

The flux q is computed at the left edge of the (+) subdomain to be passed to the (−) subdomain as a boundary condition. The discrete form of the heat-flux continuity condition at the interface ($x = v_0 t$) is thus

$$c_- \frac{T_0^{n+1} - T_0^n}{\Delta t} + c_- v_0 \frac{T_0^n - T_{-1}^n}{\Delta x_-} = \left(-q_+ - \kappa_- \frac{T_0^n - T_{-1}^n}{\Delta x_-} \right) \frac{2}{\Delta x_-} \tag{B3}$$

The flux is computed from (+) values in a first-order accurate manner as

$$q_+ = -\kappa_+ \left(\frac{T_1^n - T_0^*}{\Delta x_+} \right) \tag{B4}$$

DOI: 10.1002/fld

and is transferred as the imposed interface heat flux to the (−) subdomain

$$T_{0_*}^n = T_{0_-}^n + \frac{\Delta t}{c_+}\left(\frac{\kappa_+}{\Delta x_+^2}[T_2^{n-1} - 2T_1^{n-1} + T_{0_+}^{n-1}] - \frac{c_+ v_0}{\Delta x_+}(T_1^{n-1} - T_{0_+}^{n-1})\right.$$
$$+\omega\left\{\frac{\kappa_+}{\Delta x_+ \Delta t}[(T_1^{n-1} - T_{0_+}^{n-1}) - (T_1^{n-2} - T_{0_+}^{n-2})]\right.$$
$$\left.\left. - \frac{\kappa_-}{\Delta x_- \Delta t}[(T_{0_-}^n - T_{-1}^n) - (T_{0_-}^{n-1} - T_{-1}^{n-1})]\right\}\right) \tag{B5}$$

Combining (B3)–(B5) yields

$$c_- \frac{T_{0_-}^{n+1} - T_{0_-}^n}{\Delta t} = \frac{2}{\Delta x_-}\left\{\frac{\kappa_+}{\Delta x_+}\left[T_1^n - T_{0_-}^n - \frac{\Delta t}{c_+}\left(\frac{\kappa_+}{\Delta x_+^2}[T_2^{n-1} - 2T_1^{n-1} + T_{0_+}^{n-1}]\right.\right.\right.$$
$$-\frac{c_+ v_0}{\Delta x_+}(T_1^{n-1} - T_{0_+}^{n-1}) + \omega\left\{\frac{\kappa_+}{\Delta x_+ \Delta t}[(T_1^{n-1} - T_{0_+}^{n-1}) - (T_1^{n-2} - T_{0_+}^{n-2})]\right.$$
$$\left.\left.\left. - \frac{\kappa_-}{\Delta x_- \Delta t}[(T_{0_-}^n - T_{-1}^n) - (T_{0_-}^{n-1} - T_{-1}^{n-1})]\right\}\right)\right] - \frac{\kappa_-}{\Delta x_-}[T_{0_-}^n - T_{-1}^n]\right\}$$
$$-\frac{c_- v_0}{\Delta x_-}(T_{0_-}^n - T_{-1}^n) \tag{B6}$$

In addition to the non-dimensional parameters (21)–(23), we must define

$$\eta_\pm \equiv v_0 \frac{\Delta t}{\Delta x_\pm} \tag{B7}$$

which corresponds to the interface motion. Focusing our attention on the (−) subdomain, we solve (B1) for T_j^{n+1} and use the dimensionless parameters d_- and η_- to obtain

$$T_j^{n+1} = T_j^n + d_-(T_{j+1}^n - 2T_j^n + T_{j-1}^n) - \eta_-(T_j^n - T_{j-1}^n) \tag{B8}$$

Substituting (20) into (B8) yields

$$z = 1 + d_-(k_- - 2 + k_-^{-1}) - \eta_-(1 - k_-^{-1}) \tag{B9}$$

Applying the same steps to the (+) subdomain leads to

$$z = 1 + d_+(k_+ - 2 + k_+^{-1}) - \eta_+(1 - k_+^{-1}) \tag{B10}$$

DOI: 10.1002/fld

Turning our attention to the discretized interface equation (B6), we solve for T_0^{n+1} to obtain

$$T_{0_-}^{n+1} = T_{0_-}^n + \frac{2\Delta t}{c_-\Delta x_-}\left\{\frac{\kappa_+}{\Delta x_+}\left[T_1^n - T_{0_-}^n - \frac{\Delta t}{c_+}\left(\frac{\kappa_+}{\Delta x_+^2}[T_2^{n-1} - 2T_1^{n-1} + T_{0_+}^{n-1}]\right.\right.\right.$$
$$- \frac{c_+ v_0}{\Delta x_+}(T_1^{n-1} - T_{0_+}^{n-1}) + \omega\left\{\frac{\kappa_+}{\Delta x_+ \Delta t}[(T_1^{n-1} - T_{0_+}^{n-1}) - (T_1^{n-2} - T_{0_+}^{n-2})]\right.$$
$$\left.\left.\left. - \frac{\kappa_-}{\Delta x_- \Delta t}[(T_{0_-}^n - T_{-1}^n) - (T_{0_-}^{n-1} - T_{-1}^{n-1})]\right\}\right)\right] - \frac{\kappa_-}{\Delta x_-}[T_{0_-}^n - T_{-1}^n]\Bigg\}$$
$$- \frac{v_0 \Delta t}{\Delta x_-}(T_{0_-}^n - T_{-1}^n) \tag{B11}$$

or, in terms of the non-dimensional parameters d, η, and r,

$$T_{0_-}^{n+1} = T_{0_-}^n + 2rd_+[T_1^n - T_{0_-}^n - \theta_+(T_1^{n-1} - T_{0_+}^{n-1} - T_1^{n-2} + T_{0_+}^{n-2})$$
$$+ \frac{d_-\theta_+}{d_+ r}(T_{0_-}^n - T_{-1}^n - T_{0_-}^{n-1} + T_{-1}^{n-1}) - d_+(T_2^{n-1} - 2T_1^{n-1} + T_{0_+}^{n-1})$$
$$+ \eta_+(T_1^{n-1} - T_{0_+}^{n-1})] - 2d_-(T_{0_-}^n - T_{-1}^n) - \eta_-(T_{0_-}^n - T_{-1}^n) \tag{B12}$$

Substituting (20) into (B12) gives

$$z = 1 + 2rd_+[(k_+ - 1) - \theta_+(k_+ - 1)(z^{-1} - z^{-2}) - z^{-1}d_+(k_+^2 - 2k_+ + 1) + z^{-1}\eta_+(k_+ - 1)]$$
$$+ (1 - k_-^{-1})[2d_-\theta_+(1 - z^{-1}) - (2d_- + \eta_-)] \tag{B13}$$

Expressions (B9), (B10), and (B13) provide the three equations for the three unknowns: k_-, k_+, and z. To obtain an interface stability criterion, we solve (B9) and (B10) for k_- and k_+, respectively, and substitute the resulting expressions into (B13). Solving (B9) for k_- gives

$$k_-^{-1} = 1 - \frac{\eta_-}{d_- + \eta_-} - \frac{(1 - z - \eta_-)}{2(d_- + \eta_-)}\left[1 \mp \sqrt{1 - \frac{4d_-(1-z)}{(1 - z - \eta_-)^2}}\right] \tag{B14}$$

while (B10) yields

$$k_+ = 1 - \frac{1 - z - \eta_+}{2d_+}\left[1 \mp \sqrt{1 - \frac{4d_+(1-z)}{(1 - z - \eta_+)^2}}\right] \tag{B15}$$

From (20), we can see that the conditions $|k_+| < 1$ and $|k_-| > 1$ ensure that the temperature remains finite for $j \to \pm\infty$. These requirements are fulfilled by taking the negative signs

DOI: 10.1002/fld

in (B14) and (B15). Hence, we obtain

$$z = 1-2rd_+\left(\frac{1-z-\eta_+}{2d_+}\left[1-\sqrt{1-\frac{4d_+(1-z)}{(1-z-\eta_+)^2}}\right]\right)\left[1-\theta_+\left(\frac{1}{z}-\frac{1}{z^2}\right)\right.$$
$$\left.+\ z^{-1}d_+\left(\frac{1-z-\eta_+}{2d_+}\left[1-\sqrt{1-\frac{4d_+(1-z)}{(1-z-\eta_+)^2}}\right]\right)+z^{-1}\eta_+\right]$$
$$+\left(\frac{\eta_-}{d_-+\eta_-}+\frac{1-z-\eta_-}{2(d_-+\eta_-)}\left[1-\sqrt{1-\frac{4d_-(1-z)}{(1-z-\eta_-)^2}}\right]\right)$$
$$\times[2d_-\theta_+(1-z^{-1})-(2d_-+\eta_-)] \tag{B16}$$

For stability, it is required that $|z|<1$. Note that $z=1$ produces the trivial solution, $r<\infty$. Therefore, the stability criterion is found by inserting $z=-1$ into (B16), yielding the following inequality for stability of the CIBC coupling scheme for the moving interface case:

$$r<\frac{2+\left[\frac{\eta_-}{d_-+\eta_-}+\frac{2-\eta_-}{2(d_-+\eta_-)}\left(1-\sqrt{1-\frac{8d_-}{(2-\eta_-)^2}}\right)\right][4d_-\theta_+-(2d_-+\eta_-)]}{(2-\eta_+)\left(1-\sqrt{1-\frac{8d_+}{(2-\eta_+)^2}}\right)\left[1+2\theta_+-\eta_+-\frac{2-\eta_+}{2}\left(1-\sqrt{1-\frac{8d_+}{(2-\eta_+)^2}}\right)\right]} \tag{B17}$$

The above inequality reduces to (33) if $\eta_+=0$. Based on the analytical stability limit given by (B17), it is possible to determine the influence of interface motion in the stability of the CIBC method.

REFERENCES

1. Johnson HB, Seipp TG, Candler GV. Numerical study of hypersonic reacting boundary layer transition on cones. *Physics of Fluids* 1998; **10**(10):2676–2685.
2. Sondak SL, Dorney DJ. Simulation of coupled unsteady flow and heat conduction in turbine stage. *AIAA Journal of Propulsion and Power* 2000; **16**(6):1141–1148.
3. Lee I, Roh JH, Oh IK. Aerothermoelastic phenomena of aerospace and composite structures. *Journal of Thermal Stresses* 2003; **26**(6):525–546.
4. Armero F, Simo JC. A new unconditionally stable fractional step method for nonlinear thermomechanical problems. *International Journal for Numerical Methods in Engineering* 1992; **35**:737–756.
5. Zohdi TI. An adaptive recursive staggering strategy for simulating multi-field coupled processes in micro-heterogenous solids. *International Journal for Numerical Methods in Engineering* 2002; **53**:1511–1532.
6. Felippa CA, Park KC. Staggered transient analysis procedures for coupled mechanical systems: formulation. *Computer Methods in Applied Mechanics and Engineering* 1980; **24**:61–111.
7. Giles MB. Stability analysis of numerical interface conditions in fluid–structure thermal analysis. *International Journal for Numerical Methods in Fluids* 1997; **25**:421–436.
8. Roe B, Haselbacher A, Geubelle PH. Stability of fluid–structure thermal simulations on moving grids. *International Journal for Numerical Methods in Fluids* 2007; **54**:1097–1117.
9. Godunov SK, Ryabenkii VS. *The Theory of Difference Schemes—An Introduction*. North-Holland: Amsterdam, 1964.

DOI: 10.1002/fld

10. Blom FJ. A monolithical fluid–structure interaction algorithm applied to the piston problem. *Computer Methods in Applied Mechanics and Engineering* 1998; **167**:369–391.
11. Feng X. Analysis of finite element methods and domain decomposition algorithms for a fluid–solid interaction problem. *SIAM Journal on Numerical Analysis* 2000; **38**:1312–1336.
12. Jaiman RK, Jiao X, Geubelle PH, Loth E. Conservative load transfer along curved fluid–solid interface with nonmatching meshes. *Journal of Computational Physics* 2006; **218**:372–397.
13. Jaiman RK, Geubelle PH, Loth E, Jiao X. Stable and accurate loosely-coupled scheme for unsteady fluid–structure interaction. *AIAA Paper*, *2007–334*.
14. Strganac TW, Mook DT. Numerical model of unsteady subsonic aeroelastic behavior. *AIAA Journal* 1990; **28**: 903–909.
15. Funaro D, Quarteroni A, Zanolli P. An iterative procedure with interface relaxation for domain decomposition methods. *SIAM Journal on Numerical Analysis* 1998; **25**(6):1213–1236.
16. Rice JR, Tsompanopoulou P, Vavalis E. Interface relaxation methods for elliptic differential equations. *Applied Numerical Mathematics* 2000; **32**:219–245.
17. Richtmyer RD, Morton KW. *Difference Methods for Initial-value Problems* (2nd edn). Wiley-Interscience: New York, 1967.
18. Carslaw HS, Jaeger JC. *Conduction of Heat in Solids*. Clarendon Press: Oxford, 1959.

DOI: 10.1002/fld